Chemical Engineering Journal 506 (2025) 159543

Contents lists available at ScienceDirect

Chemical Engineering Journal

journal homepage: www.elsevier.com/locate/cej

Influence of gas composition on carbonation of quicklime granules derived from different limestone types

Katarzyna Olovsson [a,b,c], Charlie Ma [a,b], Mirva Niinipuu [d], Matias Eriksson [a,b,e], Markus Broström [a,b,*]

[a] Centre for Sustainable Cement and Quicklime Production, Department of Applied Physics and Electronics, Umeå University, SE 901 87, Umeå, Sweden
[b] Thermochemical Energy Conversion Laboratory, Department of Applied Physics and Electronics, Umeå University, SE 901 87 Umeå, Sweden
[c] Industrial Doctoral School for Research and Innovation, Umeå University, SE 901 87 Umeå, Sweden
[d] Department of Biorefinery and Energy, RISE Research Institutes of Sweden AB, 941 28 Piteå, Sweden
[e] Swedish Mineral Processing Research Association - MinFo, Marieviksgatan 25, 100 74 Stockholm, Sweden

ARTICLE INFO

Keywords:
CaO
Recarbonation
Metamorphic limestone
Sedimentary limestone
CCUS

ABSTRACT

Carbonation of quicklimes degrades their quality and can occur when process temperatures become sufficiently low. This risk can be heightened in process atmospheres containing high CO_2 and steam. To assess this, carbonation experiments involving atmospheres with different CO_2 concentrations and steam were performed at 700 °C on 2.5–5 mm quicklime granules derived from sedimentary and metamorphic limestones. The carbonation extents of the quicklimes derived from metamorphic limestones during the fast stage were higher, corresponding with their larger specific surface areas. However, SEM analysis revealed that these quicklimes had fine structures with relatively small pores that likely became blocked during carbonation, causing plateauing of carbonation that appeared to be mainly limited to particle surfaces. The presence of steam caused only mild enhancements in carbonation of these quicklimes. Contrastingly, the quicklimes derived from sedimentary limestones had lower specific surface areas that concurred with their thicker structures and larger pores. The carbonation extent during the initial fast stage was correspondingly lower, but carbonation progressed at a sustained rate thereafter. The resulting high carbonation extents appeared to be facilitated by the larger pore volumes available for carbonate growth, including locations inside particles. The presence of steam greatly enhanced the carbonation of these quicklimes. Overall, every quicklime exhibited high carbonation extents despite being granular-sized. Moreover, their distinctive carbonation behaviors and microstructures could be delineated by their parent limestone type. These findings should be considered when carbonation in high CO_2 atmospheres may occur, e.g., during cooling in electrical lime kilns.

1. Introduction

Quicklime is produced by the calcination of limestone, which is underpinned by the forwards reaction (1):

$$CaCO_3(s) \rightleftarrows CaO(s) + CO_2(g) \quad (1)$$

In order to ensure full calcination, high throughput capacity, and high final product quality, limestone is burned at 1100–1450 °C in industrial kilns. During the calcination process, around 70 % of the CO_2 emissions originate from the limestone decomposition, while 30 % originate from the burning of the fuel [1]. In 2023, more than 37.4 Gt of CO_2 was emitted from industrial processes globally [2]. That same year, approximately 430 Mt of quicklime was produced [3], emitting around 473 Mt of CO_2 [4]; this corresponded to more than 1 % of all industrial process CO_2 emissions.

The most common kiln types are rotary and shaft. A rotary kiln is horizontally oriented, with a small inclination. The most common type of rotary kiln is the Long Rotary Kiln (LRK); in this design, limestone is fed from the elevated side, while fuel and combustion air are fed from the lower end [4,5]. Shaft kilns are vertically orientated and there are several different types, the most commonly employed worldwide being the Parallel Flow Regenerative (PFR) kiln. PFR kiln design is characterized by two shafts – a burning shaft, and a non-burning (regenerative) shaft – that are connected via a channel. Fuel is fed into the burning

* Corresponding author.
E-mail address: markus.brostrom@umu.se (M. Broström).

https://doi.org/10.1016/j.cej.2025.159543
Received 25 October 2024; Received in revised form 18 December 2024; Accepted 11 January 2025
Available online 30 January 2025

shaft, and the combustion gases are transferred to the non-burning shaft. The shafts operate in these modes alternately [5,6]. Generally, a kiln consists of three temperature zones: a preheating zone, where temperatures rise from ambient up to 800 °C; a burning zone, with temperatures > 900 °C; and a cooling zone [4,6]. In a shaft kiln, the temperature of the quicklime at the cooler outlet is < 100 °C [6]. In a rotary kiln, the temperature of the quicklime at the cooler outlet has been measured to be 124 °C [7]. In conventional processes, quicklime is usually cooled with air. Integrated coolers are most commonly found in shaft kilns, while satellite, grate, and vertical coolers are most common in rotary kilns [4,8].

For successful implementation of carbon capture, utilization and storage (CCUS) systems, a high-purity CO_2 stream is needed. The use of oxygen instead of air for combustion increases the concentration of CO_2 in the flue gases, from approximately 20 vol-% to 90 vol-% [9]. Hence, the use of oxyfuel combustion has been studied in rotary kilns [10] and shaft kilns [9]. Another possible implementation of CCUS involves electrical heating of the quicklime production process. The high-purity exhaust CO_2 from an electrified calcination process can potentially be more efficient for CCUS [11,12]. However, a challenge in quicklime production processes that are intended to be used efficiently with CCUS is that the exhaust gas must not be diluted, e.g., by cooling air. Process schemes with separated gas streams for calcination and cooling have been proposed [9] but to our knowledge, they have not been implemented on an industrial scale. An alternative is to carry out the cooling with the high-CO_2 exhaust gas, but carbonation of the quicklime can lead to problems with product quality. This is represented by the backwards reaction in Eq. (1), where CaO and CO_2 react to form $CaCO_3$. For process design and optimization, detailed knowledge of carbonation reaction rates, properties of the calcinated limestone, cooling rates, and gas compositions are needed.

The carbonation reaction has been of particular interest for the Ca-looping process, in which limestone is subjected to a series of calcination-carbonation cycles wherein CaO is the CO_2 sorbent. In these studies, calcination is usually performed at 900–1000 °C and carbonation at 600–700 °C [13,14], which are efficient temperature ranges for both processes. Extensive studies have been conducted to investigate the transformation and degradation of the capture efficiency of the CaO sorbent over many cycles [15], including measures to increase the reactivity of CaO as a CO_2 sorbent [16]. The proposed reason for declining sorbent reactivity with an increasing number of cycles is the sintering of CaO during calcination [17,18]. Sintering refers to changes in pore shape and grain growth in CaO structure upon heating [15]. The specific surface area of CaO also decreases due to sintering [19]. It has been found that sintering increases with higher calcination temperatures [20], CO_2 concentrations [21–23], and steam concentrations [24], as well as in the presence of impurities [25].

Carbonation generally takes place initially as a fast, reaction-controlled step at the surface, and subsequently as a slower, diffusion-controlled process in the product layer [26,27]. The transition from fast to slow carbonation has been explained by the formation of a layer of $CaCO_3$ of a critical thickness that, when reached, decreases the rate of carbonation due to diffusion limitations [28,29]. The transition has also been attributed to pore plugging/blocking, where the formation of $CaCO_3$ in the pores of the sorbent encloses them and prevents CO_2 from reaching unreacted CaO [30–32]. Deceleration of carbonation has also been attributed to the diffusional resistance of CO_2 gas through increasingly narrow pores [33].

The influence of water vapor on the carbonation of quicklime has been studied extensively. Observed increases in quicklime carbonation in atmospheres with water vapor have been attributed to numerous factors: pore diffusion enhancement of CO_2 by H_2O [34]; solid diffusion enhancement in the product layer [35–37]; and solid diffusion enhancement via grain boundaries [33]. A proposed mechanism involves the assertion that dissociation of H_2O enables the formation of OH^- and H^+ that diffuse rapidly through $CaCO_3$ to enhance the carbonation rate [38–40]. However, depending on the carbonation conditions, steam has also been found to have no or a decelerating effect on the carbonation of quicklime [37,41–43]. The literature is therefore not conclusive about the effect of steam on the carbonation of quicklime.

The objectives of this study were three-fold. The first was to investigate the carbonation of quicklime granules. Particles in quicklime production are generally macro-sized (in the order of 10^{-3} to 1^{-1} m). While it is known that carbonation can be substantial in quicklime powders, the carbonation characteristics of larger particles are unclear. Aspects such as the lower surface-to-volume ratio and phenomena like pore plugging may play important roles in large-scale industrial processes. The second objective was to investigate the effect that moisture and CO_2 content have on the carbonation of such granules. The focus was placed on relevance to applications where high CO_2 content and moisture are likely, e.g., electrical quicklime production systems, possibly fed with wet limestone feedstocks. Hence, carbonation in 90 % CO_2 dry and humid atmospheres, after calcination in CO_2, were investigated. An atmosphere representing conventional flue gas was also used for comparison. The third objective was to establish whether carbonation is dependent on the limestone type. It is known that limestones can exhibit very different carbonation behaviors, but basic geological information about them is generally not included in published studies. To address this, four limestones were selected based on their geological classifications of sedimentary and metamorphic, and the carbonation behavior of their quicklimes was investigated. Based on pre-testing, a carbonation temperature of 700 °C was selected to meet these objectives in a concise manner.

2. Methods and Materials

2.1. Limestone materials

The experiments were performed on four limestones extracted from four different quarries. LS M−1 was extracted from a metamorphic marble quarry, where calcite marble is the dominant rock type and there are various amounts of silicates, oxides, and hydroxides. Brucite can be found along the margins, and as thin layers within the deposit. The relatively high MgO content in this limestone was also found to be in the form of dolomite, diopside and magnesian calcite. Sulfide mineralization also occurs in some parts of the quarry. LS M−2 was extracted from a crystalline metamorphic limestone quarry. Due to tectonic influence, the limestone is characterized by a shear structure with graphite-rich lamination. Accessory minerals, including amphiboles, pyrite, apatite, K-feldspar, tremolite, micas, and titanite, can be found. The microstructures of the limestones, analyzed using scanning electron microscopy (SEM), are presented in Fig. 1. LS M−1 and LS M−2 were both metamorphic limestones with a microstructure consisting of relatively large grains, often much larger than 100 μm, as shown in Fig. 1 a) and b), respectively. Metamorphic limestones are formed under high pressure and high temperature during natural geological formation processes. This leads to recrystallization and changes in the microstructure of the material [44].

LS S-1 was a sedimentary limestone extracted from a quarry rich in fossils, especially trilobite species. The limestone is quite clean in the center of the quarry, but the amount of silica increases towards the edges. LS S-2 was a sedimentary limestone extracted from a quarry characterized by horizontal layers of fossil-rich limestone and underlayers of marl. The clay minerals illite and chlorite, as well as pyrite, can be found. Dolomite crystals can be observed filling cavities and fractures, while quartz, K-feldspar, and baryte occur as accessory minerals. Fig. 1 c) and d) show the microstructures of sedimentary limestones LS S-1 and LS S-2, respectively, with typically much smaller grain sizes, many no larger than 10 μm, in contrast to the metamorphic limestones.

The chemical compositions of the limestones were ascertained using X-ray fluorescence (Panalytical Axios XRF, Malvern Panalytical, UK), and are presented as oxides in Table 1. The analysis was performed on

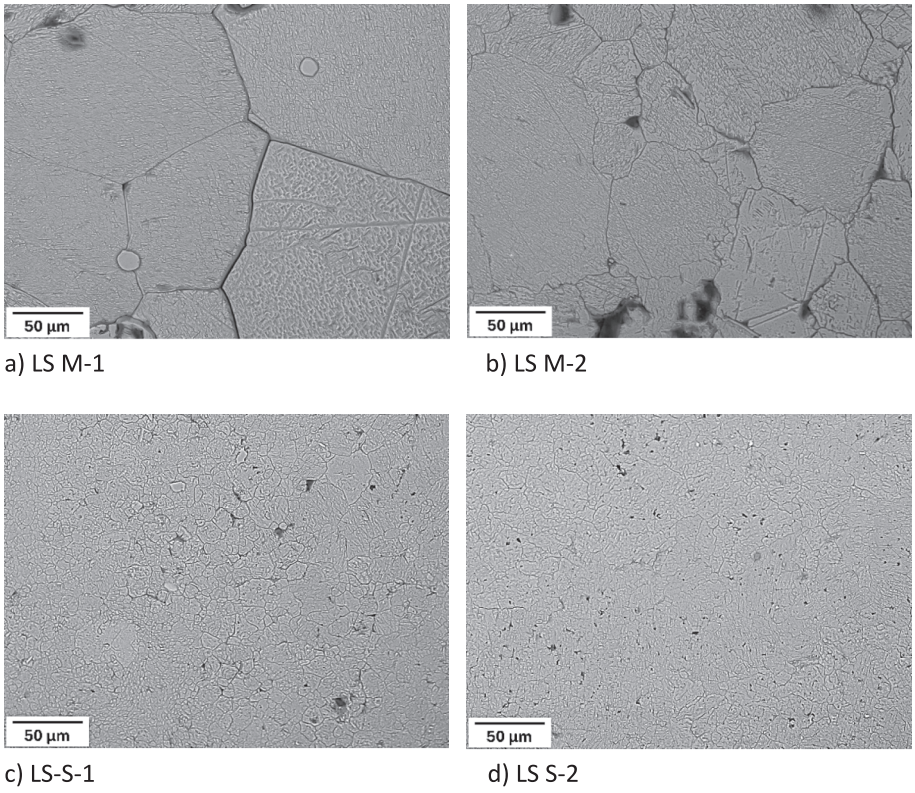

Fig. 1. SEM images of the limestone microstructures.

Table 1
The chemical composition, expressed as oxides, as ascertained using X-ray fluorescence, and LOI data for the four limestones used to produce quicklimes QL M−1, QL M−2, QL S-1, and QL S-2.

Limestone	CaO [wt.-%]	SiO_2 [wt.-%]	MgO [wt.-%]	Fe_2O_3 [wt.-%]	Al_2O_3 [wt.-%]	Σ TiO, K_2O, Na_2O, Mn_2O_3, P_2O_5 [wt.-%]	LOI [wt.-%]	Total [wt.-%]	Quicklime designation
LS M−1	48.9	4.63	4.56	0.65	1.03	0.36	39.5	99.6	QL M−1
LS M−2	54.7	0.40	0.47	0.06	0.16	0.14	43.8	99.7	QL M−2
LS S-1	54.2	1.30	0.67	0.19	0.42	0.30	43.1	100.2	QL S-1
LS S-2	53.0	1.81	1.20	0.32	0.68	0.32	42.7	100.0	QL S-2

fused beads, obtained by melting a mixture of 8 g lithium tetraborate and 0.8 g calcinated limestone in a fusion machine. Loss on ignition (LOI) analysis was performed at 950 °C. Crystallographic analysis showed that the form of calcium carbonate in every limestone was calcite.

According to classifications described elsewhere [45–47] and presented in Table S1 in Supplementary Materials, the chemical compositions indicated that LS M−2 was a high-purity limestone, LS S-1 and LS S-2 were medium- to high-purity limestones, and LS M−1 was a low-purity limestone.

Crushed samples of the limestones were sieved to collect granule-sized 2.5–5 mm fractions for the carbonation experiments. The particle size distribution is presented in Fig. S1 in Supplementary Materials. This size range is towards the lower limit of particle sizes used in rotary kilns; however, they were the largest that could be analyzed as intact granules by the surface area and pore size measurement instrument.

2.2. Macro thermogravimetric analysis

Experiments were performed in a muffle furnace (LT 9/12 SW, Nabertherm, Germany), equipped with a balance and controlled sample purge gas flow, as shown in Fig. 2.

A single layer of limestone was placed in an alumina boat, resulting in limestone samples weighing 9.85–13.85 g for each test. The boat with the material was placed in a sample cell that was purged with gas (Fig. 2). The gas flow during the calcination and carbonation runs was 1 dm^3_{STP}/min. The calcination was performed in 100 % CO_2 at a 5 °C/min heating rate up to 1000 °C with a 60 min holding time, followed by cooling in N_2 down to 700°C. After stabilizing for 10 min, the

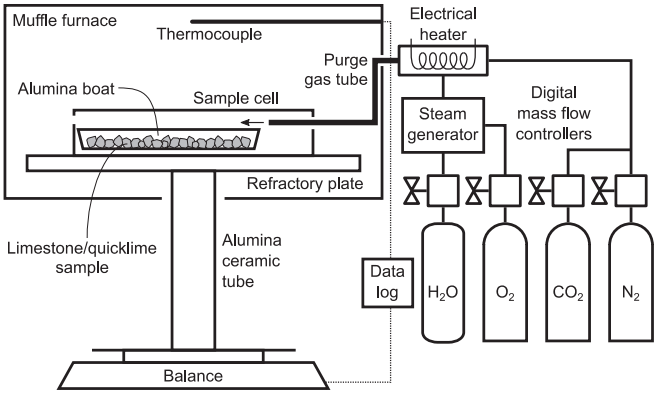

Fig. 2. The macro thermogravimetric analysis (TGA) apparatus used to calcinate limestones and perform carbonation experiments.

carbonation experiments were performed by switching the purge gas to each of the following three different atmospheres, expressed in vol.-%:

I) 90 % CO_2 and 10 % O_2 (highCO_2)
II) 90 % CO_2, 5 % H_2O, and 5 % O_2 (highCO_2 + W)
III) 30 % CO_2, 5 % O_2, 5 % H_2O, and 60 % N_2 (SimFlue)

The highCO_2 and highCO_2 + W atmospheres represented an electrified kiln with dry and wet limestone feeds, respectively, while SimFlue represented the flue gas in a conventional fuel-fired lime kiln. O_2 was added in all cases to ensure a globally completely oxidizing atmosphere.

Given that the thermodynamic $CaO/CaCO_3$ phase equilibrium at p(CO_2) = 0.3 atm is potentially as low as 790 °C [48] and that prolonged delays in carbonation can occur near the equilibrium point [49], pretesting was carried out to select an appropriate test temperature. It was found that a temperature of 700 °C could induce carbonation at reasonable rates in all the atmospheres of interest to meet the objectives concisely.

Quicklimes for further analyses were calcined under the same conditions before they were cooled down to room temperature in N_2. Quicklime and carbonated quicklime samples were kept in air-tight conditions and vacuum-cast in epoxy for SEM analysis as soon as possible after cooling. Quicklime samples were also fractured and analyzed for their microstructure without casting.

2.3. Scanning electron microscopy and energy-dispersive X-ray spectroscopy

The samples were analyzed using a Carl Zeiss Evo LS-15 SEM instrument to obtain detailed information on the microstructures. Some of the samples were cast in epoxy, grinded and polished. The grinding was performed with diamond surfaces of #120, #220, and #1200. The polishing was performed using polishing plates with 3 and 1 μm diamond solutions and an alcohol-based lubricant optimized for limestones/quicklimes. The limestone cross-sections were etched for 30 s in diluted HCl to improve grain boundary contrast. Fractured, un-cast samples were adhered onto carbon tape. The SEM was operated with an accelerating voltage of 15 keV and a 700 pA probe beam current, and imaging was carried out using a high-definition back-scattered electron detector (HDBSD). For elemental analysis, the SEM was coupled with an Oxford Instruments energy dispersive X-ray spectrometer (EDX).

2.4. BET surface area and BJH pore size distribution

The specific surface area (SSA) and pore size distribution of the quicklime sample granules were measured using the Brunauer–Emmet–Teller (BET) and Barrett–Joyner–Halenda (BJH) methods, respectively, based on multipoint N_2 adsorption/desorption isotherms obtained from a Micromeritics ASAP 2020 Plus Adsorption Analyzer (Micrometritics, Norcross, GA). Before the analysis, the samples were degassed under low vacuum (70 Pa) at 90°C for 60 min before further heating to 220 °C and holding for 120 min. 6.0 – 6.6 g of sample along with filler rods were used for analysis to ensure accuracy.

3. Results and discussion

3.1. Calcination and carbonation overview

Fig. 3 presents an example of a calcination and carbonation run. Part 1 represents heating up to 1000°C. The decomposition of impurities such as dolomite, clay minerals, and/or organic matter present in some of the limestones caused some weight loss prior to the start of calcination. The completion of calcination generally occurred during the holding time of 60 min in Part 2. During calcination, $CaCO_3$ loses around 44 % of its weight due to the release of CO_2. Part 3 represents cooling of the quicklime in N_2 down to 700 °C, where it was allowed to stabilize for 10 min. Part 4 represents carbonation in the selected atmosphere at 700 °C for 60 min, the results of which are presented and discussed below.

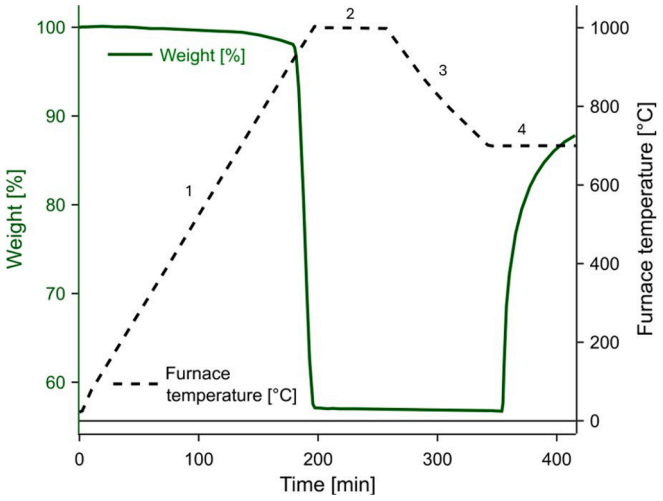

Fig. 3. TGA curves for the calcination of LS S-1 and carbonation of QL S-1 in highCO2 + W.

3.2. Carbonation analysis

Fig. 4 presents the carbonation curves for each quicklime carbonated in one of the three CO_2-containing atmospheres at 700°C for 60 min. The weight gain from carbonation relative to the starting weight of the quicklimes was calculated using the following equation (2):

$$\text{Weight gain}[\%] = \frac{(m_2 - m_1)}{m_1} * 100[\%], \quad (2)$$

where m_1 – starting weight of quicklime [g], and
m_2 – starting weight of quicklime + weight of CO_2 uptake [g]

Generally, QL S-1 and QL S-2 behaved similarly to each other, in terms of the carbonation rate and carbonation extent after 60 min, with respect to each carbonation atmosphere. QL M−1 and QL M−2 also behaved similarly to each other, but carbonation levelled out and the extents of carbonation were generally lower, especially for QL M−1.

Fig. 5 shows the corresponding carbonation rates for the quicklimes during the first 5 min. It shows that the peak carbonation rates were

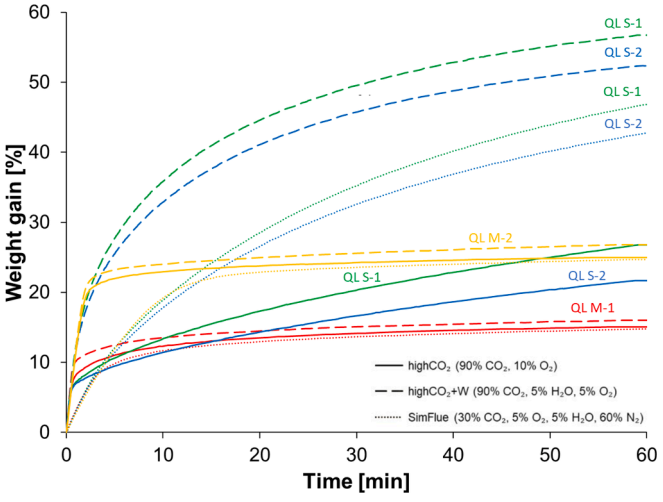

Fig. 4. The carbonation weight uptakes of CO_2 relative to the starting weight of the quicklimes, obtained at 700 °C.

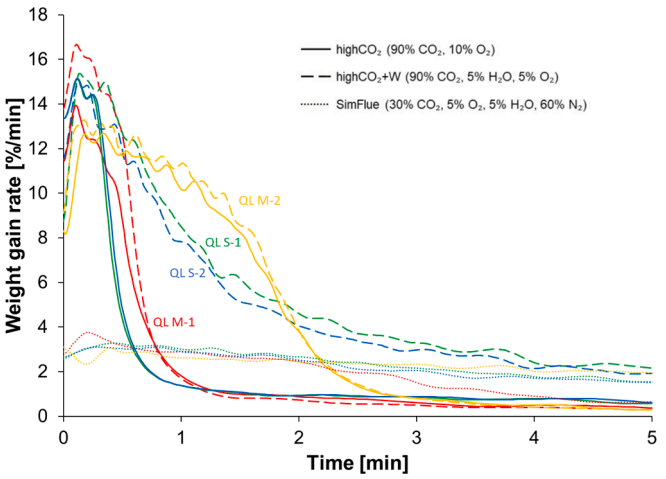

Fig. 5. Derivatives of the weight gain [%] curves shown in Fig. 4, truncated to the first 5 min.

quite similar between the quicklimes, but the rate reductions for QL M−1 and (in particular) QL M−2 were more prolonged. Over the same period in the highCO_2 + W atmosphere, carbonation was enhanced for all samples, but in different ways. While the peak rates for QL S-1 and QL S-2 did not increase significantly, the rate reduction was prolonged for these samples, such that after 2 min the sustained carbonation rate was higher than that of QL M−2. The peak carbonation rates for QL M−1 and QL M−2 increased slightly, but the rate of reduction was not enhanced compared to the highCO_2 atmosphere. This led to less carbonation extent after 5 min for QL M−1 and QL M−2 compared to QL S-1 and QL S-2. Although M−1 had a higher MgO content, only a small fraction of it constituted dolomite, which can produce quicklimes with enhanced carbonation [50,51].

In the SimFlue atmosphere, all quicklimes reached similar initial carbonation extents and rates, but the rate began to reduce more for QL M−1 after 2 min. The slower initial carbonation rate can probably be explained by the lower CO_2 concentration limiting the availability of CO_2 to the quicklimes during the first few minutes of fast carbonation.

All quicklimes showed higher carbonation extents in the highCO_2 + W atmosphere than in the highCO_2 atmosphere. This was most pronounced for QL S-1 and QL S-2, while QL M−1 and QL M−2 were much less influenced by the addition of water vapor. The weight gain curves of QL M−1 and QL M−2 flattened out to similar values in all atmospheres, while QL S-1 and QL S-2 continued CO_2 uptake at a significantly higher rate. Moreover, despite the higher CO_2 partial pressure in the highCO_2 atmosphere, the carbonation rates were lower than for the SimFlue atmosphere, vividly demonstrating the role of water vapor in sustaining carbonation in the latter. The higher carbonation rates and extents in highCO_2 + W than in SimFlue were likely the combined influence of the water vapor and higher CO_2 concentration. It was noted that the peak carbonation rate ratio for highCO_2 + W vs. SimFlue (~4–5) was greater than the CO_2 content ratio (~3.3).

3.3. *Quicklime microstructure*

Each quicklime underwent significant microstructural changes from its parent limestone (Fig. 1). Fig. 6 a) and b) show the microstructures of polished cross-sections of QL M−1 and QL M−2, respectively. Large cracks and gaps can be observed between what appear to be separated grains of their parent limestones.. These features were not observed in QL S-1 and QL S-2, shown in Fig. 6 c) and d), respectively, which seem to have remained relatively intact, despite their parent limestones possessing smaller grains. Although QL M−2 was derived from the purest limestone, the bright, elongated feature visible in the upper right corner of Fig. 6 b) indicates the presence of muscovite, based on its shape and chemical composition of K, Si, and Al.

The differences in pore microstructure between the quicklimes are presented in higher magnification SEM images of fractured particles shown in Fig. 7. The microstructures of QL M−1 and QL M−2, presented

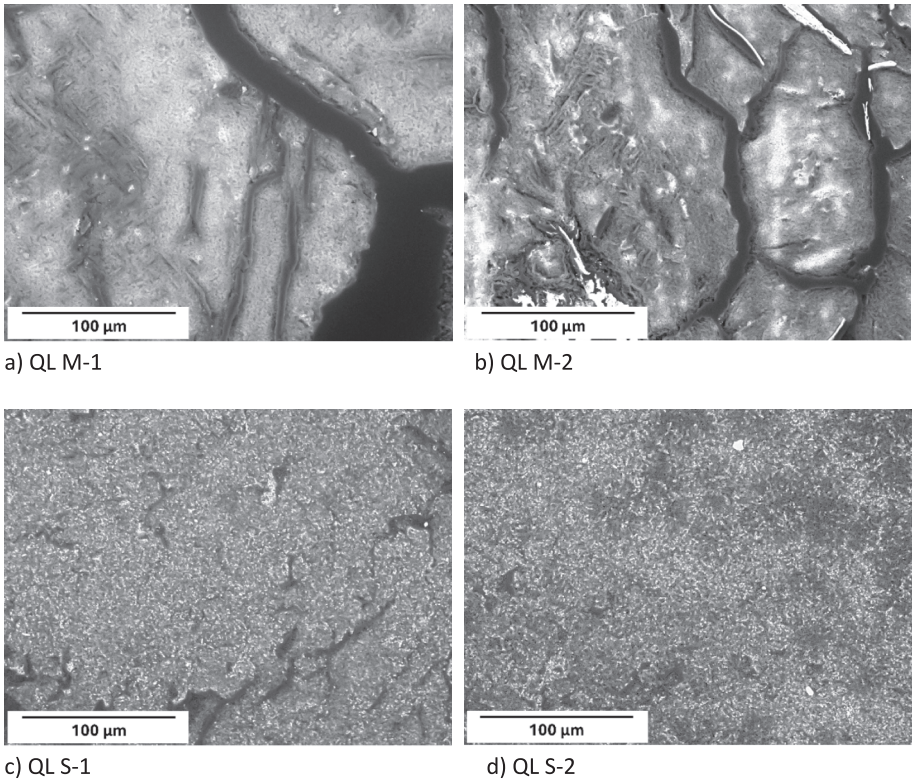

a) QL M-1 b) QL M-2

c) QL S-1 d) QL S-2

Fig. 6. SEM images of quicklime cross-sections.

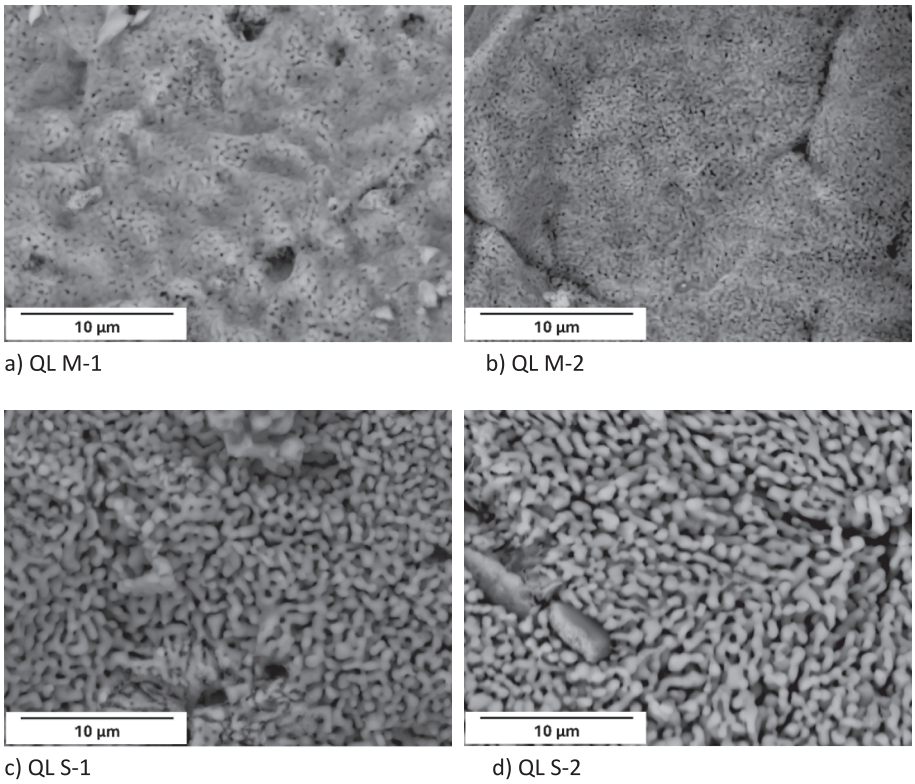

Fig. 7. SEM images of fractured surfaces of quicklimes.

in Fig. 7 a) and b), respectively, were characterized by a large number of relatively small pores (in the order of tens of nm). In contrast, the microstructures of QL S-1 and QL S-2, presented in Fig. 7 c) and d), respectively, had lower quantities of relatively large pores (in the order of hundreds of nm). The underlying solid CaO structures were also generally much thicker for QL S-1 and QL S-2 than QL M−1 and QL

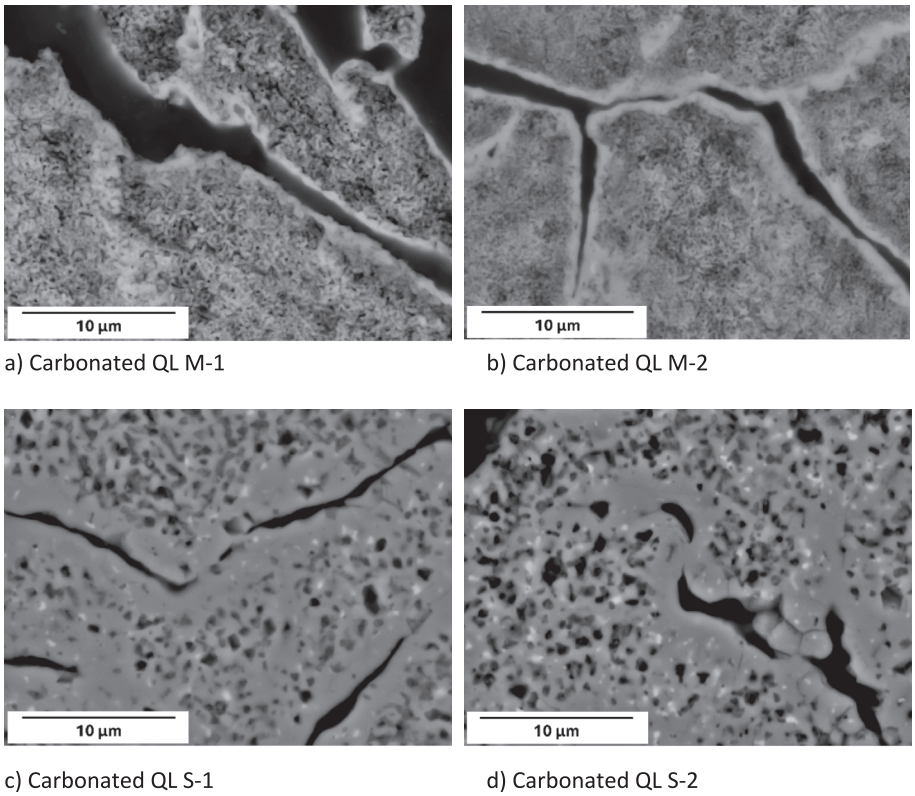

Fig. 8. SEM images of cross-sectioned and polished quicklimes carbonated in the SimFlue atmosphere.

M−2.

3.4. Carbonated quicklime microstructure

The SEM images in Fig. 8 show cross-sections of the carbonated quicklimes produced in the SimFlue atmosphere (30 % CO_2, 5 % O_2, 5 % H_2O, and 60 % N_2). As with the uncarbonated quicklimes, the microstructures of QL M−1 and QL M−2 after carbonation, shown in Fig. 8 a) and b), respectively, featured cracks that seemed to have developed between the grain boundaries of the parent limestone. Small pores reminiscent of those in the quicklimes remained in the bulk of particles, while a consolidated layer surrounded them. This appears to show that carbonation mainly occurred as a relatively thin layer on surfaces between cracks and gaps, i.e., in areas that are rapidly reached by CO_2. Carbonation did not appear to occur or progress deeply into the particles, even though the $CaCO_3$ content due to carbonation in the QL M−1 and QL M−2 samples was approximately 30 and 45 wt-%, respectively, based on the TGA measurements.

The microstructures of the cross-sectioned carbonated QL S-1 and QL S-2, shown in Fig. 8 c) and d), respectively, featured cracks between particles, and contained pores larger than those seen in carbonated QL M−1 and QL M−2. Carbonation also appears to have occurred on surfaces along the cracks, as well as inside the particles. In many instances, some resemblance of the porous structure of the quicklime can be seen deeper within the carbonated particles but thickened with carbonate growth that reduced the size of the pores. Hence, in addition to a significantly thicker carbonate layer on the surfaces of the particles, the porosity of QL S-1 and QL S-2 appears to have significantly facilitated the growth of carbonate and filling of pores within the particles. This is concordant with the relatively high amount of $CaCO_3$ present in the carbonated QL S-1 and QL S-2 samples at the end of the experiments, approximately 70 and 80 wt-%, respectively, based on the TGA measurements.

3.5. BET surface area and BJH pore size distribution

The SSA values obtained by the BET analyses and the BJH pore size distributions of the quicklimes are presented in Fig. 9. QL M−2 was the highest by a significant margin, while QL S-1 and QL S-2 possessed similarly relatively low SSAs. One of the reasons for the lower porosities and SSAs may have been sintering [23], which has been found to be accelerated by the presence of impurities [25]. LS M−2 had the lowest impurity concentration among the limestone samples, which may have led to the least sintering and highest SSA for QL M−2. Higher impurity concentrations could have caused the lower SSAs for QL S-1 and QL S-2.

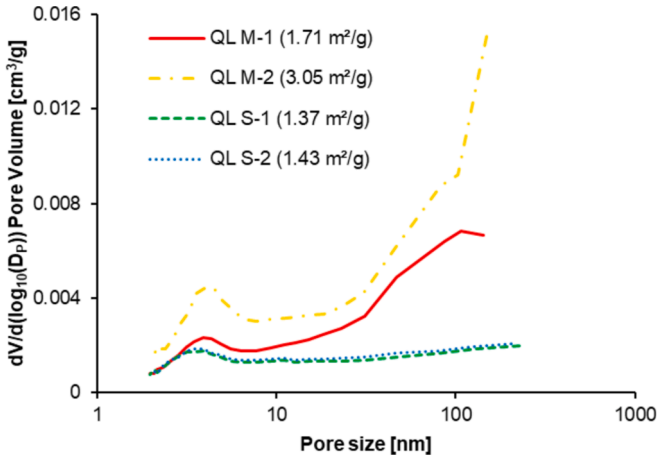

Fig. 9. Pore size distribution of the quicklimes determined by BJH method using adsorption data, and SSA from BET analysis.

In the case of QL M−1, the SEM analysis showed that it, along with QL M−2, had finer CaO structures and smaller pores compared to the quicklimes from the sedimentary limestones. Given that QL M−1 had more impurities, it is possible that they caused it to have a significantly lower SSA compared to QL M−2.

Pore sizes are classified into three categories: micropores of < 2 nm, mesopores of 2–50 nm, and macropores of > 50 nm [52,53]. QL M−1 and QL M−2 had mainly mesopores and macropores, at least up to 150 nm. In contrast, QL S-1 and QL S-2 possessed relatively few pores within the measured size range. Gas adsorption analysis has certain limitations, one being that the penetrating gas cannot enter closed pores [54]. Based on the SEM images presented in Fig. 7c) and d), the relatively large pores in QL S-1 and QL S-2 seemed to be well interconnected, but were likely too large to be determined by N_2 adsorption.

4. Further discussion

4.1. Effect of limestone type and carbonation atmosphere

The most prominent differences between the carbonation behaviors of the quicklimes, which were derived from sedimentary and metamorphic limestones, were the extents of carbonation reached during the fast stage, and the carbonation rates sustained thereafter. The carbonation extents in the fast stage corresponded to the measured SSAs of the quicklimes, i.e., QL M−2 > QL M−1 > QL S-1 ≈ QL S-2. This agrees with the assertion that carbonation during this period is only limited by the availability of surfaces that CO_2 gas can readily diffuse onto. The transition from this fast, surface-controlled stage to the slower, diffusion-controlled stage could be connected to the critical thickness of the $CaCO_3$ layer. Based on the TGA curves and SSAs of the quicklimes, the thickness of the $CaCO_3$ layer was roughly 30–40 nm for QL M−1, QL S-1, and QL S-2, and 40–50 nm for QL M−2, before carbonation transitioned to the slower, diffusion-controlled phase. These estimations of the critical layer thicknesses are within reported ranges [28].

The relative plateauing of the carbonation of the quicklimes derived from metamorphic limestones indicates severe hindrances to further carbonation beyond the fast, surface-controlled phase. The relatively small pores present in the quicklimes suggest that blockages could have occurred, preventing further ready access of CO_2 to unreacted CaO. This is supported by the observed $CaCO_3$ layer on the surfaces of the carbonated quicklimes, which is consistent with previous studies that suggest that blockage is likely to occur in narrow and fine pores [33,55]. The wider pores in the quicklimes derived from sedimentary limestones appear to have facilitated the significant carbonation rate during the diffusion-controlled stage, likely because the pores were less susceptible to blockage and provided larger spaces for $CaCO_3$ growth.

In the highCO_2 + W atmosphere, the quicklimes derived from sedimentary limestones sustained much higher rates of carbonation after the fast phase. Previous studies have proposed that steam promotes carbonation through solid state diffusion enhancement in the carbonate layer [35–37]; here, the enhancement of processes such as grain boundary diffusion may have led to the dramatic increases during the diffusion-controlled stage [56]. Others have suggested that H_2O enhances the pore diffusion of CO_2 [35]. Regardless of the mechanism, the contrastingly modest increases in carbonation observed in the quicklimes derived from metamorphic limestones indicate that such enhancements do not apply to all quicklimes. One possible explanation is that the larger pores in the quicklimes derived from sedimentary limestones allowed much more outward growth of $CaCO_3$ from the solid CaO scaffold, delaying or preventing the blockage of CO_2 and thereby also enabling carbonation to occur deeper inside particles. This is consistent with the high degree of pore filling observed in these carbonated quicklimes. Carbonation in the SimFlue atmosphere was qualitatively more similar to highCO_2 + W than highCO_2, differing mainly during the fast phase due to the lower concentration of CO_2.

The transition from surface-controlled stage of carbonation to

diffusion-controlled stage of carbonation for QL M−1 and QL M−2 was more abrupt in the highCO_2 and highCO_2 + W atmospheres than in the SimFlue atmosphere. The higher CO_2 concentrations in the highCO_2 and highCO_2 + W atmospheres reacted more quickly with QL M−1 and QL M−2, causing pore plugging to occur earlier. In contrast, the fast phase in the SimFlue atmosphere was slower, making the transition from the surface-controlled stage to the diffusion-controlled stage smoother.

4.2. Practical implications

The results presented in this study can be discussed in the context of an electrically heated quicklime production kiln, where the only expected process gases would be CO_2 and H_2O originating from limestone calcination and drying, respectively. The CO_2 concentration is higher in comparison to a conventionally heated kiln. This is especially important for the cooling zone of the kiln, where quicklime undergoes a temperature decrease and the presence of CO_2 and water vapor can result in the carbonation of quicklime. An important finding is that, despite being in granular form, all of the investigated quicklimes exhibited propensity to carbonate to a significant extent. Although the quicklimes derived from metamorphic limestones exhibited signs of pore blockage during carbonation, the carbonation extent reached was substantial. Cracks formed at what appeared to be between the grain boundaries of the parent limestone, suggesting that carbonation may still be significant even if larger particles are present, because such cracks facilitate CO_2 access.

According to industrial requirements, quicklime with $CaCO_3$ content exceeding 3 wt-% is considered to be low quality. The results showed that in the highCO_2 and highCO_2 + W atmospheres, the carbonate content in the quicklime exceeded 3 wt-% during the initial 5–10 s of carbonation (see Figs. S2 a) and b), supplementary material). In the SimFlue atmosphere, the carbonate content was above this threshold in 30 s. During an actual cooling process, carbonation of the quicklime can, in principle, begin once the temperature drops below the conditions required for thermodynamic equilibrium. In dry, high-CO_2 atmospheres, quicklimes with higher surface areas, i.e., those derived from metamorphic limestones, likely carbonate significantly more than ones with lower surface areas, i.e., those derived from sedimentary limestones, in the same timeframe. While the quicklimes derived from the sedimentary limestones carbonated to a greater extent after a significant amount of time under the tested isothermal conditions, under cooling conditions it is possible that carbonation would cease in these materials before it reaches the level of carbonation of the metamorphic counterparts due to the reduction in reaction kinetics. However, the presence of water vapor can dramatically enhance the carbonation of quicklimes derived from sedimentary limestones. Hence, the type of limestone feed needs careful consideration in future electrically heated kilns, as do the process conditions. In addition, the distinctive differences in carbonation behavior and microstructures of the quicklimes derived from the different limestone types motivate for further studies to elucidate their calcination-carbonation cycling behavior, which is of interest in Ca-looping processes.

5. Conclusions

The carbonation behavior of four granular quicklimes derived from metamorphic and sedimentary limestones were experimentally investigated in three different CO_2-containing atmospheres at 700 °C for 60 min. The resulting carbonation rates and extents varied depending on both the limestone type and atmosphere.

During the initial fast, surface-controlled phase of carbonation occurred, the dry 90 % CO_2 atmosphere caused the quicklimes derived from metamorphic limestones to reach higher carbonation extents than the quicklimes derived from sedimentary limestones. This was in agreement with specific surface area measurements of the quicklimes.

The carbonation of quicklimes derived from both sedimentary and metamorphic limestones was enhanced by the addition of steam, but the effect was much more pronounced for the quicklimes derived from sedimentary limestones. The differences in quicklime microstructure suggest that pore size played a role in determining the carbonation behavior. The quicklimes derived from metamorphic limestones were characterized by particles separated by cracks, and relatively fine pores that could be blocked by formed $CaCO_3$. Carbonation seems to have occurred mainly as relatively thin layers along the surfaces of these particles. On the other hand, the quicklimes derived from sedimentary limestones were characterized by thicker structures and larger pores that were likely less susceptible to blockage. However, carbonate formation seemed extensive enough to fill some of these larger pores in addition to forming a thick layer on the surfaces of the particles, resulting in comparatively high levels of carbonation.

In general, the quicklimes derived from sedimentary limestones behaved similarly to each other, with carbonation progressing at similarly high rates until the end of the experiments. The quicklimes derived from metamorphic limestones also behaved similarly to each other, with the carbonation extents relatively levelling out within a short period. The final carbonation weight uptakes of the quicklimes derived from metamorphic limestones were generally lower than those of the quicklimes derived from sedimentary limestones, despite the more rapid initial carbonation of the former.

CRediT authorship contribution statement

Katarzyna Olovsson: Writing – review & editing, Writing – original draft, Investigation, Formal analysis, Data curation, Conceptualization. **Charlie Ma:** Writing – review & editing, Supervision, Investigation, Formal analysis, Data curation, Conceptualization. **Mirva Niinipuu:** Writing – review & editing, Investigation, Data curation. **Matias Eriksson:** Writing – review & editing, Supervision, Project administration, Funding acquisition, Conceptualization. **Markus Broström:** Writing – review & editing, Supervision, Project administration, Funding acquisition, Conceptualization.

Declaration of competing interest

The authors declare that they have no known competing financial interests or personal relationships that could have appeared to influence the work reported in this paper.

Acknowledgements

Nordkalk AB, SMA Mineral AB, Heidelberg Materials Cement Sverige AB, the Ellen, Walter and Lennart Hesselman Foundation, the Swedish Mineral Processing Research Association – MinFo, the Swedish Energy Agency and Sweden's innovation agency Vinnova are acknowledged for their project support. This project has also received funding from the European Union's Horizon Europe research and innovation programme under Grant Agreement No 101138392. The authors acknowledge the facilities and technical assistance of the Umeå Core Facility Electron Microscopy (UCEM) at the Chemical Biological Centre (KBC), Umeå University.

Appendix A. Supplementary data

Supplementary data to this article can be found online at https://doi.org/10.1016/j.cej.2025.159543.

Data availability

Data will be made available on request.

References

[1] M. Stork, W. Meindertsma, M. Overgaag, M. Neelis, A Competitive and Efficient Lime Industry, EuLA - The European Lime Association, 2014.
[2] International Energy Agency, CO2 emissions in 2023, Report, 2023.
[3] U.S. Geological Survey, Mineral commodity summaries, 2024.
[4] F. Schorcht, I. Kuorti, B.M. Scalet, S. Roudier, S.L. Delgado, Best Available Techniques (BAT) Reference Document for the Production of Cement, Lime and Magnesium Oxide, Joint Reasearch Centre of the European Comission, Seville, Spain, 2013.
[5] M. Simoni, M.D. Wilkes, S. Brown, J.L. Provis, H. Kinoshita, T. Hanein, Decarbonising the lime industry: State-of-the-art, Renew. Sustain. Energy Rev. 168 (2022) 112765.
[6] H. Piringer, Lime Shaft Kilns INFUB - 11th European Conference on Industrial Furnaces and Boilers, Energy Procedia, 2017, pp. 75-95.
[7] H. Shahin, S. Hassanpour, A., Saboonchi Thermal energy analysis of a lime production process: Rotary kiln, preheater and cooler, Energ. Conver. Manage. 114 (2016) 110–121.
[8] R.S. Boynton, Chemistry and Technology of Lime and Limestone., Second, Edition ed., Wiley Interscience, New York, 1980.
[9] H. Piringer, P. Bucher, R. Wallimann, Sustainable lime burning technology with shaft kilns, ZKG 6 (2021) 34–41.
[10] M. Eriksson, B. Hökfors, R. Backman, Oxyfuel combustion in rotary kiln lime production, Energy Sci. Eng. 2 (4) (2014) 204–215.
[11] B. Wilhelmsson, R. Backman, Reducing the CO2 footprint of cement production by electrification, 15th International Congress on the Chemistry of Cement Prague, Czech Republic, 2019.
[12] N. Macdowell, N. Florin, A. Buchard, J. Hallett, A. Galindo, G. Jackson, C. S. Adjiman, C.K. Williams, N. Shah, P. Fennell, An overview of CO2 capture technologies, Energ. Environ. Sci. 3 (11) (2010) 1645.
[13] A. Lasheras, J. Ströhle, A. Galloy, B. Epple, Carbonate looping process simulation using a 1D fluidized bed model for the carbonator, Int. J. Greenhouse Gas Control 5 (2011) 686–693.
[14] M. Romano, Coal-fired power plant with calcium oxide carbonation for postcombustion CO2 capture, Energy Procedia 1 (2009) 1099–1106.
[15] J. Blamey, E.J. Anthony, J. Wang, P.S. Fennell, The calcium looping cycle for large-scale CO2 capture, Prog. Energy Combust. Sci. 36 (2) (2010) 260–279.
[16] M. Erans, V. Manovic, E.J. Anthony, Calcium looping sorbents for CO2 capture, Appl. Energy 180 (2016) 722–742.
[17] G.S. Grasa, J.C. Abanades, CO2 capture capacity of CaO in long series of carbonation/calcination cycles, Ind. Eng. Chem. Res. 45 (26) (2006) 8846–8851.
[18] V. Manovic, E.J. Anthony, Steam reactivation of spent CaO-based sorbent for multiple CO2 capture cycles, Environ. Sci. Tech. 41 (2007) 1420–1425.
[19] R.H. Borgwardt, Calcination kinetics and surface area of dispersed limestone particles, AIChE Journal 31 (1) (1985) 103–111.
[20] C. Wang, X. Zhou, L. Jia, Y. Tan, Sintering of limestone in calcination/carbonation cycles, Ind. Eng. Chem. Res. 53 (42) (2014) 16235–16244.
[21] F. Rubiera, A.B. Fuertes, J.J. Pis, V. Artos, G. Marban, Changes in textural properties of limestone and dolomite during calcination, Thermochim Acta 179 (1991) 125–134.
[22] J.M. Valverde, P.E. Sanchez-Jimenez, L.A. Perez-Maqueda, Limestone calcination nearby equilibrium: kinetics, CaO crystal structure, sintering and reactivity, J. Phys. Chem. 119 (2015) 1623–1641.
[23] D. Beruto, L. Barcco, CO2-catalyzed surface area and porosity changes in high-surface-area CaO aggregates, J. Am. Ceram. Soc. 67 (1984) 512–515.
[24] R.H. Borgwardt, Calcium oxide sintering in atmospheres containing water and carbon dioxide, Ind. Eng. Chem. Res. 28 (1989) 493–500.
[25] R.H. Borgwardt, Sintering of nascent calcium oxide, Chem. Eng. Sci. 44 (1989) 53–60.
[26] S.K. Bhatia, D.D. Perlmutter, Effect of the product layer on the kinetics of the CO2-lime reaction, AIChE Journal 29 (1) (1983) 79–86.
[27] R. Barker, The reversibility of the reaction CaCO3 ⇄ CaO+CO2, J. Appl. Chem. Biotech. 23 (10) (1973) 733–742.
[28] D. Alvarez, J.C. Abanades, Determination of the critical product layer thickness in the reaction of CaO with CO2, Ind. Eng. Chem. Res. 44 (2005) 5608–5615.
[29] G. Grasa, R. Murillo, M. Alonso, J.C. Abanades, Application of the random pore model to the carbonation cyclic reaction, AIChE J 55 (5) (2009) 1246–1255.
[30] M. Benitez-Guerrero, J.M. Valverde, P.E. Sanchez-Jimenez, A. Perejon, L.A. Perez-Maqueda, Multicycle activity of natural CaCO3 minerals for thermochemical energy storage in Concentrated Solar Power plants, Sol. Energy 153 (2017) 188–199.
[31] J.J. Arcenegui Troya, P.E. Sanchez-Jiménez, A. Perejón, V. Moreno, J.M. Valverde, L.A. Pérez-Maqueda, Kinetics and cyclability of limestone (CaCO3) in presence of steam during calcination in the CaL scheme for thermochemical energy storage, Chem. Eng. J. 417 (2021) 129194.
[32] A.A. Scaltsoyiannes, A.A. Lemonidou, On the factors affecting the deactivation of limestone under calcium looping conditions: A new comprehensive model, Chem. Eng. Sci. 243 (2021) 116797.
[33] M.T. Dunstan, F. Donat, A.H. Bork, C.P. Grey, C.R. Muller, CO2 Capture at medium to high temperature using solid oxide based sorbents: fundamental aspects, mechanistic insights, and recent advances, Chem. Rev. 121 (2021) 12681–12745.
[34] F. Donat, N.H. Florin, E.J. Anthony, P.S. Fennell, Influence of High-Temperature Steam on the Reactivity of CaO Sorbent for CO2 Capture, Environ. Sci. Tech. 46 (2) (2012) 1262–1269.
[35] V. Manovic, E.J. Anthony, Carbonation of CaO-based sorbents enhanced by steam addition, Ind. Eng. Chem. Res. 49 (19) (2010) 9105–9110.
[36] A. Coppola, E. Gais, G. Mancino, F. Montagnaro, F. Scala, P. Salatino, Effect of steam on the performance of Ca-based sorbents in calcium looping processes, Powder Technol. 316 (2017) 578–584.
[37] J.J. Arcenegui Troya, V. Moreno, P.E. Sanchez-Jiménez, A. Perejón, J.M. Valverde, L.A. Pérez-Maqueda, Effect of steam injection during carbonation on the multicyclic performance of limestone (CaCO3) under different calcium looping conditions: a comparative study, ACS Sustain. Chem. Eng. 10 (2) (2022) 850–859.
[38] Z. Li, Y. Liu, N. Cai, Understanding the enhancement effect of high-temperature steam on the carbonation reaction of CaO with CO2, Fuel 127 (2014) 88–93.
[39] Z.-H. Li, Y. Wang, K. Xu, J.-Z. Yang, S.-B. Niu, H.Y. Shao-Bo, Effect of steam on CaO regeneration, carbonation and hydration reactions for CO2 capture, Fuel Process. Technol. 151 (2016) 101–106.
[40] Y. Fan, J.G. Yao, Z. Zhang, M. Sceats, Y. Zhuo, L. Li, G.C. Maitland, P.S. Fennell, Pressurized calcium looping in the presence of steam in a spout-fluidizedbed reactor with DFT analysis, Fuel Process. Technol. 169 (2018) 24–41.
[41] B. Arias, G. Grasa, J.C. Abanades, V. Manovic, E.J. Anthony, The effect of steam on the fast carbonation reaction rates of CaO, Ind. Eng. Chem. Res. 51 (5) (2012) 2478–2482.
[42] P. Sun, J.R. Grace, C.J. Lim, E.J. Anthony, Investigation of attempts to improve cyclic CO_2 capture by sorbent hydration and modification, Ind. Eng. Chem. Res. 47 (2008) 2024–2032.
[43] I. Lindén, P. Backman, A. Brink, M. Hupa, Influence of water vapor on carbonation of CaO in the temperature range 400–550 °C, Ind. Eng. Chem. Res. 50 (24) (2011) 14115–14120.
[44] K. Bucher, M. Frey, Petrogenesis of Metamorphic Rocks, 7th ed., Springer Verlag, Berlin, 2002.
[45] C. Mitchell, High purity limestone quest, British Geological Survey (2011).
[46] F.C. Cox, D.M. Bridge, J.H. Hull, Procedure fot the assessment of limestone resources, London, 1977.
[47] D.J. Harrison, K.A.M. Adlam, Limestones of the peak: A guide to the limestone and dolomite resources of the Peak District of Derbyshire and Staffordshire, British Geological Survey (1985).
[48] C.W. Bale, E. Belisle, P. Chartrand, S.A. Decterov, G. Eriksson, A.E. Gheiribi, K. Hack, I.-H. Jung, Y.-B. Kang, J. Melancon, A.D. Pelton, S. Peterson, C. Robelin, J. Sangster, P. Spencer, M.-A. Van Ende, FactSage thermochemical software and databases, 2010–2016, Calphad 54 (2016) 35–53.
[49] C. Ortiz, J. Valverde, R. Chacartegui, L. Perez-Maqueda, Carbonation of limestone derived CaO for thermochemical energy storage: From kinetics to process integration in concentrating solar plants, ACS Sustain. Chem. Eng. 6 (2018) 6404–6417.
[50] A. De La Calle Martos, J.M. Valverde, P.E. Sanchez-Jimenez, A. Perejón, C. García-Garrido, L.A. Perez-Maqueda, Effect of dolomite decomposition under CO2 on its multicycle CO2 capture behaviour under calcium looping conditions, PCCP 18 (24) (2016) 16325–16336.
[51] J.M. Valverde, P.E. Sanchez-Jimenez, L.A. Perez-Maqueda, Ca-looping for postcombustion CO2 capture: A comparative analysis on the performances of dolomite and limestone, Appl. Energy 138 (2015) 202–215.
[52] L. Wu, Y. Li, Z. Fu, B.L. Su, Hierarchically structured porous materials: synthesis strategies and applications in energy storage, Natl. Sci. Rev. 7 (2020) 1667–1701.
[53] International Union of Pure and Applied Chemistry, Reporting Physiosorption Data for Gas/Solid Systems, Pure Appl. Chem. (1985) 603–619.
[54] S.T. Ho, D.W. Hutmacher, A comparison of micro CT with other techniques used in the characterization of scaffolds, Biomaterials 27 (2006) 1362–1376.
[55] S.L. Homsy, J. Moreno, A. Dikhtiarenko, J. Gascon, R.W. Dibble, Calcium Looping: On the Positive Influence of SO2 and the Negative Influence of H2O on CO2 Capture by Metamorphosed Limestone-Derived Sorbents, ACS Omega 5 (50) (2020) 32318–32333.
[56] Z. Li, H. Sun, N. Cai, Rate Equation Theory for the Carbonation Reaction of CaO with CO2, Energy Fuel 26 (2012) 4607–4616.